Integrated Plasmonics: Broadband Dirac Plasmons in Borophene

Chao Lian,[1] Shi-Qi Hu,[1,2] Jin Zhang,[1,2] Cai Cheng,[1] Zhe Yuan,[3] Shiwu Gao,[4,*] and Sheng Meng[1,2,5,†]
[1]*Beijing National Laboratory for Condensed Matter Physics and Institute of Physics, Chinese Academy of Sciences, Beijing 100190, China*
[2]*University of Chinese Academy of Sciences, Beijing 100049, China*
[3]*Center for Advanced Quantum Studies and Department of Physics, Beijing Normal University, Beijing 100875, China*
[4]*Beijing Computational Science Research Center, Beijing 100193, China*
[5]*Songshan Lake Materials Laboratory, Dongguan, Guangdong 523808, China*

(Received 4 June 2019; revised 30 August 2019; accepted 12 August 2020; published 9 September 2020)

The past decade has witnessed numerous discoveries of two-dimensional (2D) semimetals and insulators, whereas 2D metals were rarely identified. Borophene, a monolayer boron sheet, has recently emerged as a perfect 2D metal with unique electronic properties. Here we study collective excitations in borophene, which exhibit two major plasmon modes with low damping rates extending from the infrared to ultraviolet regime. The anisotropic 1D plasmon originates from electronic transitions of tilted Dirac cones in borophene, analogous to that in extreme doped graphene. These features enable borophene as an integrated platform of 1D, 2D, and Dirac plasmons, promising for directional polariton transport and broadband optical communication in next-generation optoelectronic devices.

DOI: 10.1103/PhysRevLett.125.116802

When propagating along the metal-dielectric interface, electromagnetic waves couple with electronic motions and form surface plasmon polaritons (SPPs) [1,2]. Noble metal films (e.g., Ag and Au) provide abundant free electrons to generate high-frequency plasmons in SPP devices [3–6]. However, the SPPs in these devices suffer from low confinement and significant losses during propagation [7–9], resulting from the manifold interband damping and strong plasmon-phonon scatterings [10,11].

Naturally, ultrathin two-dimensional (2D) materials, such as graphene [12–16], phosphorene [17–21], and MoS_2 [22–28], are proposed to generate SPPs with low damping rates and high confinements due to stronger light-matter interactions [29–46]. However, low carrier densities in these materials limit the frequencies of plasmonic response up to terahertz or infrared region, where light sources and optoelectronic detectors are less developed [47–53]. The 2D materials with higher carrier density and higher plasmon frequencies are particularly desirable for building optical devices for beyond-diffraction-limit resolution, biotechnological detection, and enhancing atomic transitions [54–57].

Recently, borophene, a monolayer boron sheet, has been experimentally synthesized either on a solid substrate via molecular beam epitaxy [58,59] or as freestanding atomic sheets via sonochemical liquid-phase exfoliation [60]. Borophene has extraordinary electric, optical, and transport properties, which are highly related to its intrinsic metallic, Dirac-type band structures [61–68]. The density of the Dirac electrons in borophene is extremely high (10^{15} e/cm^2) [61–63] compared to doped graphene ($10^{12} \sim 10^{14}$ e/cm^2) [69]. Thus, we expect that borophene, as an intrinsic 2D metal with both a high carrier density and high confinement, can be a promising candidate to build low-loss broadband SPP devices.

In this Letter, we report discovery of low-loss and highly confined broadband plasmons in borophene, based on time-dependent density functional theory (TDDFT) [70,78]. We identify two plasmon branches: A high-energy (HE) mode extends to ultraviolet and originates from collective excitations of bulk electrons in the 2D metal; in the low-energy (LE) region, a new plasmon mode exhibits a strong anisotropic behavior and broadband response. This new plasmon mode originates from collective electronic transitions of one-dimensional (1D) electron gas derived from tilted Dirac cones. Both modes show remarkable low-loss properties comparable to graphene, but at significant higher frequencies, thanks to borophene's high carrier density and low-dimension nature [11]. The confinement of plasmon in borophene is also 2–3 orders of magnitude higher than that in Ag [7]. The discovery of novel plasmon modes make borophene more suitable than graphene and noble metals for plasmon generation and integrated optoelectronics working at a broad range of frequencies.

Figure 1 shows the atomic structure of the β_{12} borophene. The β_{12} borophene is the most stable phase found in experiments [58–60] and is thus chosen as a representative structure of borophene. The unit cell is rectangular with the lattice parameters $a_1 = 2.92$ and $a_2 = 5.06$ Å, consisting of five boron atoms. Periodic vacancies line up along the horizontal direction (denoted as the X direction). This special structure introduces

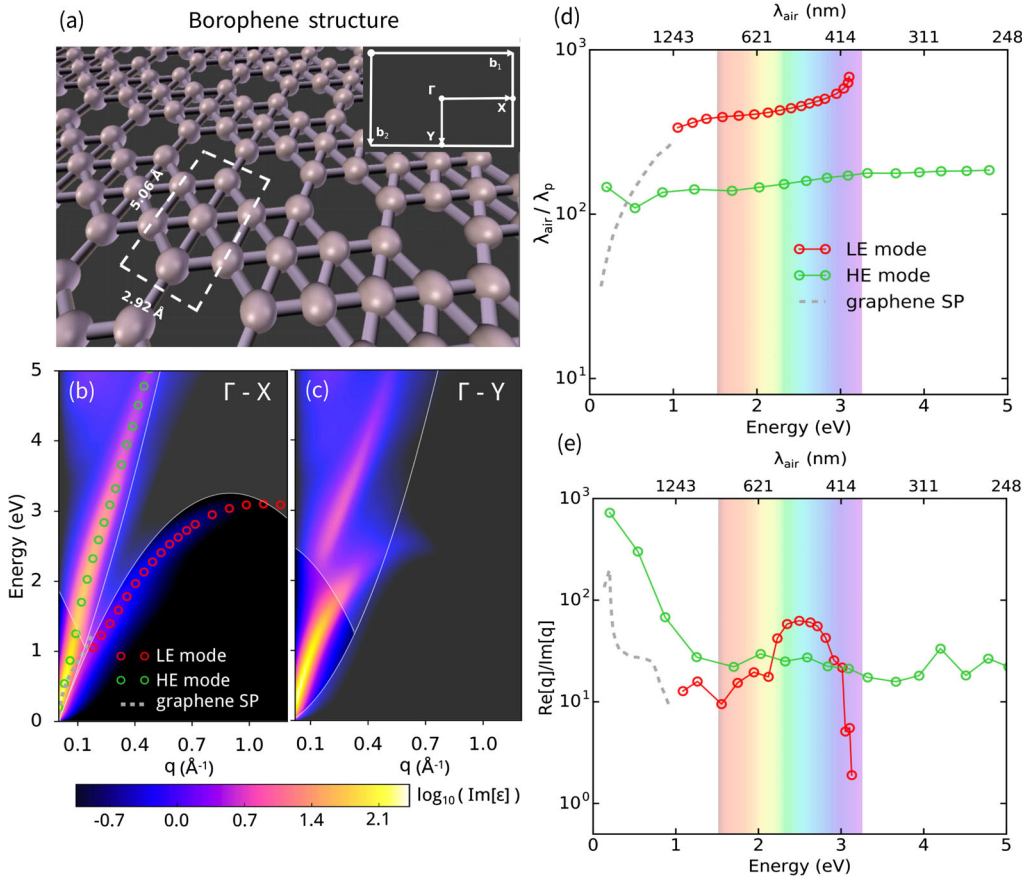

FIG. 1. (a) Structure and Brillouin zone of β_{12} borophene. (b),(c) Imaginary parts of dielectric functions along the $\Gamma - X$ and $\Gamma - Y$ directions. Shaded areas denote the SPE regions. Green and red circles denote the peaks of the HE and LE mode, respectively. The dashed line in (b) represents the dispersion of surface plasmon (SP) in graphene [11]. (d) Confinement ratio $\lambda_{\mathrm{air}}/\lambda_p$ and (e) loss $\mathrm{Re}[q]/\mathrm{Im}[q]$ of borophene and graphene plasmon as a function of wavelength. The carrier density in doped graphene is set as $n = 3 \times 10^{13}$ cm^{-2}. The colored areas denote the energy range of the visible light with the corresponding color.

anisotropy between the horizontal (X) and vertical (Y) directions in both the real and reciprocal space [Fig. 1(a)].

The optical absorption spectra, obtained from the imaginary part of the dielectric function (see Supplemental Material [78]), are shown in Figs. 1(b) and 1(c). We observe two broad plasmon branches in different energy ranges in our calculations. The high-energy branch disperses almost linearly and extends to the ultraviolet regime. This mode is almost isotropic along the X and Y directions. In contrast, the low-energy branch shows evident anisotropic dispersions. Along the $\Gamma - X$ direction, the LE branch shows an inverted parabolic dispersion over the whole Brillouin zone, with the maximum energy at half of the reciprocal lattice vector, $q = |\mathbf{b_1}|/2 = 1.07$ Å^{-1}. Along the Γ-Y, however, only the HE mode shows up at small q regimes; the LE mode develops only at energies higher than ~2 eV, whereas the two plasmon modes strongly hybridize with each other.

Both the HE and LE branches can form a broadband SPP with low losses. As shown in Figs. 1(d) and 1(e), we calculate the confinement ratio $\lambda_{\mathrm{air}}/\lambda_p$ and relative loss $\mathrm{Re}[q]/\mathrm{Im}[q]$ of borophene plasmons, where λ_{air} and λ_p are the light wavelengths in air and borophene, respectively [11]. The LE plasmons possess high confinement ratios $\lambda_{\mathrm{air}}/\lambda_p$ of 330–700 and large $\mathrm{Re}[q]/\mathrm{Im}[q]$ of 10–700 at different wavelengths from 400 to 1240 nm. The $\lambda_{\mathrm{air}}/\lambda_p$ and $\mathrm{Re}[q]/\mathrm{Im}[q]$ of the HE plasmon are slightly lower over a broader energy range. Both the confinement ratios and losses are comparable to those in heavily doped graphene ($\lambda_{\mathrm{air}}/\lambda_p \sim 300$ and $\mathrm{Re}[q]/\mathrm{Im}[q] = 10$–$200$) [11] and much larger than those in the Al or Ag films ($\lambda_{\mathrm{air}}/\lambda_p \approx 1$) [7]. Furthermore, the low damping SPPs only exists within the infrared regime ($\lambda_{\mathrm{air}} > 1240$ nm) in graphene [11,14,18,28], while borophene can generate the low-loss SPPs in a much broader energy range from infrared to ultraviolet. This indicates that borophene is a better building material for the low-loss broadband opto-electronic devices.

We discuss the electronic origin of these two outstanding characteristics, the anisotropy and low-loss rate, of the borophene plasmon. We first note that the anisotropic plasmon in borophene is *not* a trivial consequence of the

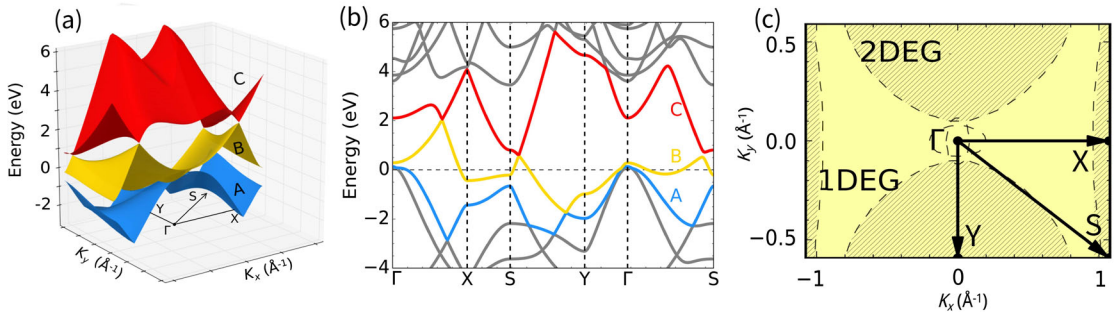

FIG. 2. (a) Three- and (b) two-dimensional band structure, and (c) the Fermi surface of β_{12} borophene.

rectangular lattice, which generates only a weak anisotropy in phosphorene plasmons [18]. Instead, the unique electronic structure is the major reason of the anisotropy. As shown in Figs. 2(a) and 2(b), band B crosses the Fermi energy and joins band C at the Dirac points at 2 eV, indicating the metallic nature of borophene and forming the Fermi surface shown in Fig. 2(c). Another Dirac point forms along the S–Y direction and at a lower energy, 0.5 eV. Both Dirac cones are tilted in their shape, consistent with experimental measurements [61,62]. Thus, borophene forms a Fermi surface comprising three parts: (I) a ribbon along $\Gamma - Y$ centered at X, implying a 1D electron gas (1DEG) from tilted Dirac electrons subjecting to strong confinement along the Y direction; (II) two semicircular regions characterizing a bulk 2D electron gas; (III) a small hole pocket near the Γ point.

We ascribe the anisotropic LE mode to the intraband oscillations of the 1DEG between the Dirac cones. As shown in Fig. 3, we analyze the contributions of different electron-hole transitions to the plasmonic peaks within the independent particle approximation (IPA). As shown in Figs. 3(a)–3(c), the HE mode emerges mainly at ~3.8 eV for $q = 0.36$ Å^{-1}, which comes from mixed interband transitions between bands $A \to B$, $A \to C$, and $B \to C$. In comparison, the LE peaks are located at 1.08, 1.79, and 0.5 eV for $q = 0.18$, 0.36, and 2.06 Å^{-1}, respectively, which are dominated by the intraband transitions $B \to B$. Accordingly, we visualize the excitation mode of the LE plasmon in the reciprocal space. The contour plot of the energy difference, $\omega_{B,B}(q, \mathbf{k})$, between the initial state $\{B, \mathbf{k} - \mathbf{q}\}$ and final state $\{B, \mathbf{k}\}$, where $\omega_{B,B}(q, \mathbf{k}) = \epsilon_{B\mathbf{k}} - \epsilon_{B\mathbf{k}-\mathbf{q}}$ for $\epsilon_{B\mathbf{k}} > 0 \bigcap \epsilon_{B\mathbf{k}-\mathbf{q}} < 0$, and $\epsilon_{B\mathbf{k}}$ is the

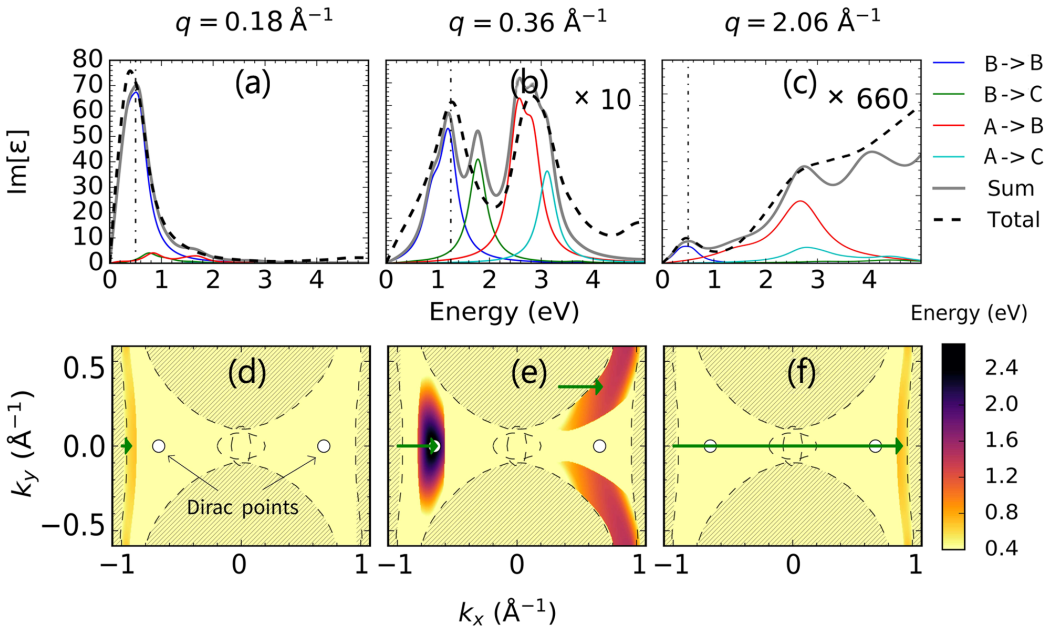

FIG. 3. (a)–(c) Imaginary part of the dielectric function at different momenta q. Transition $X \to Y$ denotes the component contributed by excitations from band X to Y ($X, Y \in \{A, B, C\}$) [see Figs. 2(a) and 2(b)]. Gray lines denote the sum of contributions by the excitation from band X to Y ($X, Y \in \{A, B, C\}$) for (a) and (b), while for (c) excitations between $\{A, B, C\}$ and five higher bands are also included. (d)–(f) The contour plot of the energy difference for $B \to B$ intraband transition $\omega_{B,B}(q, k) = \epsilon_{B,k} - \epsilon_{B,k-q}$ at different q. The green arrows denote the excitation from $k - q$ to k. Gray dashed lines denote the Fermi surface.

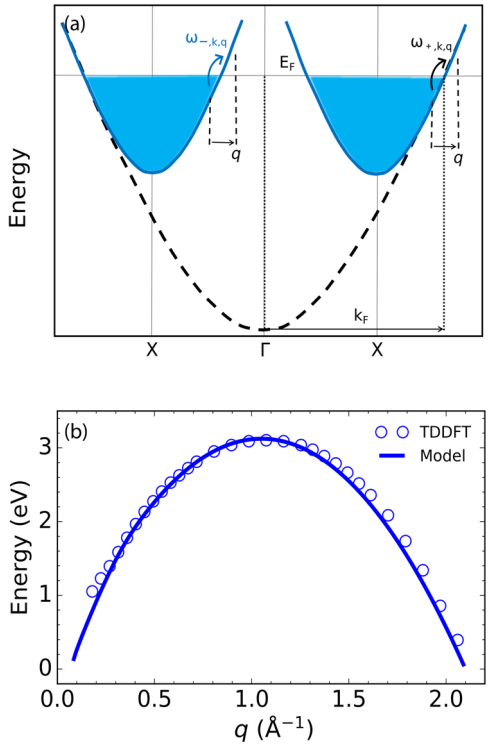

FIG. 4. (a) Schematic band structure along $X-\Gamma-X$. The dashed line follows $E_k = k^2/2m^* + E_0$ with $E_0 = -3.26$ eV and $m^* = 1.6m_0$, representing the band of 1DEG@Γ with the same dispersion as that of 1DEG@X. The black and blue arrows denote the excitation channel of 1DEG@Γ and 1DEG@X, respectively. (b) The LE plasmon dispersions calculated by the 1DEG model (solid line) and TDDFT (open circles).

eigenvalue of band B at the $\mathbf{k}$ point. As shown in Figs. 3(d)–3(f), the oscillation of the 1DEG dominates the LE mode and leads to its anisotropy, since the 1DEG can only oscillate along $\Gamma-X$ direction. Specifically, at $q = 0.36$ Å^{-1}, the LE plasmon is generated by electron excitations from the Fermi surface to the Dirac points [61]. Thus, borophene can be viewed as an extremely hole-doped graphene in generating the LE plasmon.

To explain the mechanism of the low-damping characteristic, we adopt the confined 1DEG model [89–91] that is widely used to describe plasmons of atomic chains [92–97]. We find an additional excitation channel exists in the borophene for its special 1DEG centered at X point (1DEG@X), compared with the usual 1DEG@Γ: For excitations at certain momentum q, the conventional channel for 1DEG@Γ [the black arrow in Fig. 4(a)] is $\omega_{+,k,q} = \omega_{k+q} - \omega_k = (kq + \frac{1}{2}q^2)/m$, with $\omega_k = k^2/2m$ (assuming $\hbar = 1$ and m is the effective mass of electron). For 1DEG@X, there is an additional channel (the blue arrow) located on the opposite side ($-k_F$) $\omega_{-,k,q} = \omega_{-k+q} - \omega_{-k} = (-kq + \frac{1}{2}q^2)/m$.

Accordingly, we calculate the plasmon dispersions of these two excitation channels, which are determined from the zeros of the dielectric function $\epsilon(q,\omega_p) = 1 - V(q)\mathrm{Re}\chi_0(q,\omega_p) = 0$. Here, ω_p is the frequency of plasmon, $V(q)$ is the Coulomb potential, χ_0 is the response function with IPA [98] $\chi_0(q,\omega_p) = (1/\pi)\int dk\theta(q \pm k - k_F)\theta(k_F \mp k)\{[1/(\omega - \omega_{\pm,k,q} + i\eta)] - [1/(\omega + \omega_{\pm,k,q} + i\eta)]\}$. Thus, $\mathrm{Re}\chi_0(q,\omega_p) = \pm(1/\pi q)\ln[(\omega^2 - \omega_-^2)/(\omega^2 - \omega_+^2)]$, where $\omega_\pm^2 = |k_F q \pm \frac{1}{2}q^2|/m$ are the upper (+) and lower (−) limits of the single-particle excitation (SPE) regimes, respectively. The 1D plasmon dispersions can be solved as $\omega_p^+(q) = \sqrt{[A(q)\omega_+^2 - \omega_-^2]/[A(q)-1]}$ and $\omega_p^-(q) = \sqrt{[A(q)\omega_-^2 - \omega_+^2]/[A(q)-1]}$ [89,98], where $A(q) = \exp\{\pi q/[mV(q)]\}$, $V(q) = e^2/Ke^{b^2q^2}\int_{b^2q^2}^{\infty} e^{-x}/x dx$, K is the static dielectric constant, b is the width of the 1DEG, and m is the effective mass of electrons the 1DEG.

As shown in Fig. 4(b), while $\omega_p^+(q)$ hybridizes and merges with the isotropic HE mode, $\omega_p^-(q)$ accurately reproduces the inverse parabolic dispersion calculated from TDDFT, with the parameters $k_F = 1.07$ Å^{-1}, $b = 4$ Å, $K = 6.25$, and $m = 2.4m_0$. We note that, among the parameters, k_F is the length of $\Gamma - X$ and thus not adjustable; 1DEG width b and dielectric constant K have negligible effects on $\omega_p(q)$ when $q > 0.1$ Å^{-1}. The effective mass $m = 2.4m_0$ is slightly larger than that evaluated from the band structure $m^* = 1.6m_0$, due to many body screening effects. This indicates that our model directly and robustly reflects the electronic origin of novel borophene plasmon.

The same model may also explain the LE plasmon branch along the $\Gamma - Y$ direction. Along $\Gamma - Y$, electrons first undergo an interband excitation to energy levels at ~2 eV above the Fermi level, where electrons form a similar 1DEG confined along $\Gamma - Y$ direction. With strong interband transitions included in plasmon excitations, excitations of the 1DEG at $\Gamma - Y$ have similar excitation channels as 1DEG along $\Gamma - X$ discussed above. Therefore, a kink in plasmon dispersion at ~2 eV is formed, followed by an inverse parabolic dispersion along the $\Gamma - Y$ direction.

Based on these results, we discuss the mechanism of the low-damping behavior of the LE plasmon. With $q \to \infty$, these two branches $\omega_p^-(q)$ and $\omega_p^+(q)$ yield different asymptotic behaviors. The $A(q)$ dominates when $q \to \infty$ and leads $\omega_p^+(q) \to \omega_+$ and $\omega_p^-(q) \to \omega_-$. That is, $\omega_p^+(q)$ [$\omega_p^-(q)$] is always higher (lower) than the SPE region. Moreover, the Dirac-type intraband excitations [Fig. 3(e)] further suppress the SPE region, since the pseudospin symmetry forbids perpendicularly polarized excitations [30]. The combined effects remarkably produce the low-loss LE plasmons.

We briefly discuss technical requirements for building realistic plasmonic devices with borophene. The first important requirement is the stability of borophene under ambient conditions. Feng *et al.* showed that a borophene

sheet on the Ag substrate remains intact when exposed to oxygen gas, and air with oxidation mainly occurs at the edges [59]. Ranjan *et al.* synthesized large-scale freestanding borophene by liquid-phase exfoliation [60], claiming that freestanding borophene layers are stable against oxidation. This indicates that a borophene-based device in ambient condition is applicable. Other than stability, large-scale high-quality borophene sheets are needed for device applications. We note that local point defects in borophene barely affect its overall band structures (Fig. S4, Supplemental Material [78]). Furthermore, charge doping has little effect on the plasmonic response of borophene (Fig. S3, Supplemental Material [78]). Thus, borophene plasmon is insensitive to defects and dopants in low concentrations, similar to the experimental results observed in graphene [99,100]. However, anisotropic plasmon responses will probably be substantially smeared in polycrystalline borophene. Synthesis of centimeter-scale single-crystalline borophene is needed for building plasmonic borophene devices, which is quite promising considering recent breakthroughs in the growth of wafer-scale graphene [101,102], transition metal dichalcogenides [103], and boron nitride [104]. We expect that the unique plasmon properties predicted here will motivate further experimental efforts to prepare high-quality borophene samples and novel plasmonic devices.

Absent in other 2D materials, we observe in our calculations the coexistence and interplay of the 1DEG, 2DEG, and Dirac electrons in the collective plasmon excitations in metallic borophene. The exotic features such as low-loss, strong confinement, and panchromatic responses of LE and HE plasmons make borophene an integrated platform for applications in nanophotonics and optoelectronics working at broadband frequencies.

We acknowledge insightful discussions with Professor Ling Lu. This work is partially supported by MOST (Grant No. 2016YFA0300902), NSFC (Grants No. 11774396 and No. 91850120), and CAS (XDB330301). S. G. acknowledges supports from MOST through Grants No. 2017YFA0303404 and No. 2016YFB0700701, NSFC through Grants No. 11934003, No. U1930402, and No. 21961132023.

C. L. and S. H. contributed equally to this work.

*swgao@csrc.ac.cn
†smeng@iphy.ac.cn

[1] J. M. Pitarke, V. M. Silkin, E. V. Chulkov, and P. M. Echenique, Rep. Prog. Phys. **70**, 1 (2007).
[2] S. A. Maier, *Plasmonics: Fundamentals and Applications* (Springer, New York, 2007).
[3] Y. Gao, Z. Yuan, and S. Gao, J. Chem. Phys. **134**, 134702 (2011).
[4] S. Thongrattanasiri, A. Manjavacas, and F. J. G. de Abajo, ACS Nano **6**, 1766 (2012).
[5] P. Sessi, V. M. Silkin, I. A. Nechaev, T. Bathon, L. El-Kareh, E. V. Chulkov, P. M. Echenique, and M. Bode, Nat. Commun. **6**, 8691 (2015).
[6] X. Zubizarreta, E. V. Chulkov, I. P. Chernov, A. S. Vasenko, I. Aldazabal, and V. M. Silkin, Phys. Rev. B **95**, 235405 (2017).
[7] R. Sundararaman, T. Christensen, Y. Ping, N. Rivera, J. D. Joannopoulos, M. Soljai, and P. Narang, Phys. Rev. Mater. **4**, 074011 (2020).
[8] G. Slotman, A. Rudenko, E. van Veen, M. I. Katsnelson, R. Roldán, and S. Yuan, Phys. Rev. B **98**, 155411 (2018).
[9] N. Rivera, I. Kaminer, B. Zhen, J. D. Joannopoulos, and M. Soljačić, Science **353**, 263 (2016).
[10] P. West, S. Ishii, G. Naik, N. Emani, V. Shalaev, and A. Boltasseva, Laser Photonics Rev. **4**, 795 (2010).
[11] M. Jablan, H. Buljan, and M. Soljačić, Phys. Rev. B **80**, 245435 (2009).
[12] T. Low and P. Avouris, ACS Nano **8**, 1086 (2014).
[13] F. J. G. de Abajo, ACS Photonics **1**, 135 (2014).
[14] S. N. Shirodkar, M. Mattheakis, P. Cazeaux, P. Narang, M. Soljačić, and E. Kaxiras, Phys. Rev. B **97**, 195435 (2018).
[15] G. X. Ni, A. S. McLeod, Z. Sun, L. Wang, L. Xiong, K. W. Post, S. S. Sunku, B.-Y. Jiang, J. Hone, C. R. Dean, M. M. Fogler, and D. N. Basov, Nature (London) **557**, 530 (2018).
[16] R. Yu, Q. Guo, F. Xia, and F. J. García de Abajo, Phys. Rev. Lett. **121**, 057404 (2018).
[17] T. Low, R. Roldán, H. Wang, F. Xia, P. Avouris, L. M. Moreno, and F. Guinea, Phys. Rev. Lett. **113**, 106802 (2014).
[18] B. Ghosh, P. Kumar, A. Thakur, Y. S. Chauhan, S. Bhowmick, and A. Agarwal, Phys. Rev. B **96**, 035422 (2017).
[19] S. Saberi-Pouya, T. Vazifehshenas, T. Salavati-fard, and M. Farmanbar, Phys. Rev. B **96**, 115402 (2017).
[20] L. C. Gomes and A. Carvalho, Phys. Rev. B **92**, 085406 (2015).
[21] E. van Veen, A. Nemilentsau, A. Kumar, R. Roldn, M. I. Katsnelson, T. Low, and S. Yuan, Phys. Rev. Applied **12**, 014011 (2019).
[22] A. Scholz, T. Stauber, and J. Schliemann, Phys. Rev. B **88**, 035135 (2013).
[23] W. Liu, B. Lee, C. H. Naylor, H.-S. Ee, J. Park, A. T. C. Johnson, and R. Agarwal, Nano Lett. **16**, 1262 (2016).
[24] B. Yue, F. Hong, K.-D. Tsuei, N. Hiraoka, Y.-H. Wu, V. M. Silkin, B. Chen, and H. K. Mao, Phys. Rev. B **96**, 125118 (2017).
[25] H. S. Sen, L. Xian, F. H. daJornada, S. G. Louie, and A. Rubio, Isr. J. Chem. **57**, 540 (2017).
[26] W. Liu, B. Lee, C. H. Naylor, H.-S. Ee, J. Park, A. T. C. Johnson, and R. Agarwal, Nano Lett. **16**, 1262 (2016).
[27] J. Miao, W. Hu, Y. Jing, W. Luo, L. Liao, A. Pan, S. Wu, J. Cheng, X. Chen, and W. Lu, Small **11**, 2392 (2015).
[28] Z. Torbatian and R. Asgari, J. Phys. Condens. Matter **29**, 465701 (2017).
[29] S. D. Sarma and A. Madhukar, Phys. Rev. B **23**, 805 (1981).

[30] E. H. Hwang and S. D. Sarma, Phys. Rev. B **75**, 205418 (2007).
[31] Z. Yuan and S. Gao, Surf. Sci. **602**, 460 (2008).
[32] S. Dai, Q. Ma, M. K. Liu, T. Andersen, Z. Fei, M. D. Goldflam, M. Wagner, K. Watanabe, T. Taniguchi, M. Thiemens, F. Keilmann, G. C. A. M. Janssen, S.-E. Zhu, P. Jarillo-Herrero, M. M. Fogler, and D. N. Basov, Nat. Nanotechnol. **10**, 682 (2015).
[33] J. D. Cox, I. Silveiro, and F. J. G. de Abajo, ACS Nano **10**, 1995 (2016).
[34] Z. Fei, A. S. Rodin, G. O. Andreev, W. Bao, A. S. McLeod, M. Wagner, L. M. Zhang, Z. Zhao, M. Thiemens, G. Dominguez, M. M. Fogler, A. H. C. Neto, C. N. Lau, F. Keilmann, and D. N. Basov, Nature (London) **487**, 82 (2012).
[35] M. Polini, R. Asgari, G. Borghi, Y. Barlas, T. Pereg-Barnea, and A. H. MacDonald, Phys. Rev. B **77**, 081411 (R) (2008).
[36] J. Chen, M. Badioli, P. Alonso-González, S. Thongrattanasiri, F. Huth, J. Osmond, M. Spasenović, A. Centeno, A. Pesquera, P. Godignon, A. Z. Elorza, N. Camara, F. J. G. de Abajo, R. Hillenbrand, and F. H. L. Koppens, Nature (London) **487**, 77 (2012).
[37] D. Ansell, I. P. Radko, Z. Han, F. J. Rodriguez, S. I. Bozhevolnyi, and A. N. Grigorenko, Nat. Commun. **6**, 8846 (2015).
[38] F. J. G. de Abajo, ACS Photonics **1**, 135 (2014).
[39] F. Xia, H. Wang, D. Xiao, M. Dubey, and A. Ramasubramaniam, Nat. Photonics **8**, 899 (2014).
[40] A. Thakur, R. Sachdeva, and A. Agarwal, J. Phys. Condens. Matter **29**, 105701 (2017).
[41] C. Vacacela Gomez, M. Pisarra, M. Gravina, J. M. Pitarke, and A. Sindona, Phys. Rev. Lett. **117**, 116801 (2016).
[42] L. Marušić and V. Despoja, Phys. Rev. B **95**, 201408(R) (2017).
[43] J. Yan, K. W. Jacobsen, and K. S. Thygesen, Phys. Rev. B **84**, 235430 (2011).
[44] V. Despoja and L. Marušić, Phys. Rev. B **97**, 205426 (2018).
[45] M. Jung, Z. Fan, and G. Shvets, Phys. Rev. Lett. **121**, 086807 (2018).
[46] A. Politano, G. Chiarello, B. Ghosh, K. Sadhukhan, C.-N. Kuo, C. S. Lue, V. Pellegrini, and A. Agarwal, Phys. Rev. Lett. **121**, 086804 (2018).
[47] Y. Gao and Z. Yuan, Solid State Commun. **151**, 1009 (2011).
[48] F. H. L. Koppens, D. E. Chang, and F. J. G. de Abajo, Nano Lett. **11**, 3370 (2011).
[49] T. Low and P. Avouris, ACS Nano **8**, 1086 (2014).
[50] T. Low, A. Chaves, J. D. Caldwell, A. Kumar, N. X. Fang, P. Avouris, T. F. Heinz, F. Guinea, L. Martin-Moreno, and F. Koppens, Nat. Mater. **16**, 182 (2017).
[51] V. W. Brar, M. S. Jang, M. Sherrott, J. J. Lopez, and H. A. Atwater, Nano Lett. **13**, 2541 (2013).
[52] V. W. Brar, M. S. Jang, M. Sherrott, S. Kim, J. J. Lopez, L. B. Kim, M. Choi, and H. Atwater, Nano Lett. **14**, 3876 (2014).
[53] G. X. Ni, L. Wang, M. D. Goldflam, M. Wagner, Z. Fei, A. S. McLeod, M. K. Liu, F. Keilmann, B. zyilmaz, A. H. C. Neto, J. Hone, M. M. Fogler, and D. N. Basov, Nat. Photonics **10**, 244 (2016).
[54] J. D. Cox and F. J. G. de Abajo, Phys. Rev. Lett. **121**, 257403 (2018).
[55] D. Gérard and S. K. Gray, J. Phys. D **48**, 184001 (2015).
[56] C. M. Soukoulis and M. Wegener, Nat. Photonics **5**, 523 (2011).
[57] J. B. Pendry, Phys. Rev. Lett. **85**, 3966 (2000).
[58] A. J. Mannix, X.-F. Zhou, B. Kiraly, J. D. Wood, D. Alducin, B. D. Myers, X. Liu, B. L. Fisher, U. Santiago, J. R. Guest, M. J. Yacaman, A. Ponce, A. R. Oganov, M. C. Hersam, and N. P. Guisinger, Science **350**, 1513 (2015).
[59] B. Feng, J. Zhang, Q. Zhong, W. Li, S. Li, H. Li, P. Cheng, S. Meng, L. Chen, and K. Wu, Nat. Chem. **8**, 563 (2016).
[60] P. Ranjan, T. K. Sahu, R. Bhushan, S. S. Yamijala, D. J. Late, P. Kumar, and A. Vinu, Adv. Mater. **31**, e1900353 (2019).
[61] B. Feng, O. Sugino, R.-Y. Liu, J. Zhang, R. Yukawa, M. Kawamura, T. Iimori, H. Kim, Y. Hasegawa, H. Li, L. Chen, K. Wu, H. Kumigashira, F. Komori, T.-C. Chiang, S. Meng, and I. Matsuda, Phys. Rev. Lett. **118**, 096401 (2017).
[62] B. Feng, J. Zhang, S. Ito, M. Arita, C. Cheng, L. Chen, K. Wu, F. Komori, O. Sugino, K. Miyamoto, T. Okuda, S. Meng, and I. Matsuda, Adv. Mater. **30**, 1704025 (2018).
[63] J. Zhang, J. Zhang, L. Zhou, C. Cheng, C. Lian, J. Liu, S. Tretiak, J. Lischner, F. Giustino, and S. Meng, Angew. Chem. Int. Ed. **57**, 4585 (2018).
[64] B. Feng, J. Zhang, R.-Y. Liu, T. Iimori, C. Lian, H. Li, L. Chen, K. Wu, S. Meng, F. Komori, and I. Matsuda, Phys. Rev. B **94**, 041408(R) (2016).
[65] Y. Zhao, S. Zeng, and J. Ni, Appl. Phys. Lett. **108**, 242601 (2016).
[66] E. S. Penev, A. Kutana, and B. I. Yakobson, Nano Lett. **16**, 2522 (2016).
[67] Z. Jalali-Mola and S. A. Jafari, Phys. Rev. B **98**, 235430 (2018).
[68] Y. Huang, S. N. Shirodkar, and B. I. Yakobson, J. Am. Chem. Soc. **139**, 17181 (2017).
[69] D. K. Efetov and P. Kim, Phys. Rev. Lett. **105**, 256805 (2010).
[70] The frequency- and wave-vector-dependent density response functions are calculated within the TDDFT formalism using random-phase approximation as implemented in the GPAW package [71–75]. The projector augmented-waves method and Perdew-Burke-Ernzerhof exchange-correlation [76] are used for the ground state calculations. The plane-wave cutoff energy is set to be 500 eV. The thickness of vacuum layer is set to be larger than 10 Å. The Brillouin zone is sampled using the Monkhorst-Pack scheme [77] with a dense **k**-point mesh $142 \times 72 \times 1$ in the self-consistent calculations.
[71] J. J. Mortensen, L. B. Hansen, and K. W. Jacobsen, Phys. Rev. B **71**, 035109 (2005).
[72] J. Enkovaara *et al.*, J. Phys. Condens. Matter **22** 253202 (2010).
[73] J. Yan, J. J. Mortensen, K. W. Jacobsen, and K. S. Thygesen, Phys. Rev. B **83**, 245122 (2011).
[74] A. H. Larsen *et al.*, J. Phys. Condens. Matter **29** 273002 (2017).

[75] S. R. Bahn and K. W. Jacobsen, in *Computing in Science & Engineering* (IEEE, New York, 2002), pp. 56–66, https://ieeexplore.ieee.org/abstract/document/998641/authors.
[76] J. P. Perdew, K. Burke, and M. Ernzerhof, Phys. Rev. Lett. **77**, 3865 (1996).
[77] Hendrik J. Monkhorst and James D. Pack, Phys. Rev. B **13**, 5188 (1976).
[78] See Supplemental Material at http://link.aps.org/supplemental/10.1103/PhysRevLett.125.116802 for details of additional method details, data, discussions, and figures, which includes Refs. [79–88].
[79] J. P. Perdew and A. Zunger, Phys. Rev. B **23**, 5048 (1981).
[80] S. Sharma, J. K. Dewhurst, A. Sanna, and E. K. U. Gross, Phys. Rev. Lett. **107**, 186401 (2011).
[81] G. Giuliani and G. Vignale, *Quantum Theory of the Electron Liquid* (Cambridge University Press, Cambridge, England, 2005).
[82] M. Corradini, R. Del Sole, G. Onida, and M. Palummo, Phys. Rev. B **57**, 14569 (1998).
[83] M. A. L. Marques, C. A. Ullrich, F. Nogueira, A. Rubio, K. Burke, and E. K. U. Gross, *Time-Dependent Density Functional Theory* (Springer, Berlin, Heidelberg, 2006).
[84] M. Cazzaniga, H.-C. Weissker, S. Huotari, T. Pylkkänen, P. Salvestrini, G. Monaco, G. Onida, and L. Reining, Phys. Rev. B **84**, 075109 (2011).
[85] N. Wiser, Phys. Rev. **129**, 62 (1963).
[86] P. V. C. Medeiros, S. Stafström, and J. Björk, Phys. Rev. B **89**, 041407(R) (2014).
[87] P. V. C. Medeiros, S. S. Tsirkin, S. Stafström, and J. Björk, Phys. Rev. B **91**, 041116(R) (2015).
[88] C. Lian and S. Meng, Phys. Rev. B **95**, 245409 (2017).
[89] S. D. Sarma and E. H. Hwang, Phys. Rev. B **54**, 1936 (1996).
[90] S. Gao and Z. Yuan, Phys. Rev. B **72**, 121406(R) (2005).
[91] J. Yan, Z. Yuan, and S. Gao, Phys. Rev. Lett. **98**, 216602 (2007).
[92] J. J. Ritsko, D. J. Sandman, A. J. Epstein, P. C. Gibbons, S. E. Schnatterly, and J. Fields, Phys. Rev. Lett. **34**, 1330 (1975).
[93] E. P. Rugeramigabo, C. Tegenkamp, H. Pfnür, T. Inaoka, and T. Nagao, Phys. Rev. B **81**, 165407 (2010).
[94] T. Nagao, S. Yaginuma, T. Inaoka, and T. Sakurai, Phys. Rev. Lett. **97**, 116802 (2006).
[95] J. Yan and S. Gao, Phys. Rev. B **78**, 235413 (2008).
[96] C. Liu, T. Inaoka, S. Yaginuma, T. Nakayama, M. Aono, and T. Nagao, Phys. Rev. B **77**, 205415 (2008).
[97] C. Liu, T. Inaoka, S. Yaginuma, T. Nakayama, M. Aono, and T. Nagao, Nanotechnology **19**, 355204 (2008).
[98] W. I. Friesen and B. Bergersen, J. Phys. C **13**, 6627 (1980).
[99] A. Politano, A. R. Marino, V. Formoso, D. Farías, R. Miranda, and G. Chiarello, Phys. Rev. B **84**, 033401 (2011).
[100] T. Langer, J. Baringhaus, H. Pfnr, H. W. Schumacher, and C. Tegenkamp, New J. Phys. **12**, 033017 (2010).
[101] Y. Lee, S. Bae, H. Jang, S. Jang, S.-E. Zhu, S. H. Sim, Y. I. Song, B. H. Hong, and J.-H. Ahn, Nano Lett. **10**, 490 (2010).
[102] Y.-M. Lin, A. Valdes-Garcia, S.-J. Han, D. B. Farmer, I. Meric, Y. Sun, Y. Wu, C. Dimitrakopoulos, A. Grill, P. Avouris, and K. A. Jenkins, Science **332**, 1294 (2011).
[103] C. Liu, L. Wang, J. Qi, and K. Liu, Adv. Mater. **32**, 2000046 (2020).
[104] L. Wang *et al.*, Nature (London) **570**, 91 (2019).